International Journal of Heat and Mass Transfer 51 (2008) 5226–5237

Contents lists available at ScienceDirect

International Journal of Heat and Mass Transfer

journal homepage: www.elsevier.com/locate/ijhmt

Onset of entrainment in transitional round fountains

Wenxian Lin [a,c,*], S.W. Armfield [b]

[a] Solar Energy Research Institute, Yunnan Normal University, Kunming, Yunnan 650092, PR China
[b] School of Aerospace, Mechanical and Mechatronic Engineering, The University of Sydney, NSW 2006, Australia
[c] School of Engineering, James Cook University, Townsville, QLD 4811, Australia

ARTICLE INFO

Article history:
Received 12 September 2007
Received in revised form 28 February 2008
Available online 5 May 2008

Keywords:
Transitional fountain
Entrainment
Direct numerical simulation
Turbulent flow

ABSTRACT

It is of fundamental interest to understand the behavior of transitional fountains with intermediate Froude and Reynolds numbers, together with the associated entrainment and turbulence. In this work, the transient behavior of axisymmetric fountains with $1 \leqslant Fr \leqslant 8$ and $200 \leqslant Re \leqslant 800$ is studied by direct numerical simulation. It is found that at $Re \leqslant 200$, there is little entrainment present at the upflow–downflow interface and at the downflow–ambient interface, even for a value of Fr as high as 8; however, at $Re > 200$, entrainment is present at these interfaces and the extent increases with Re, which clearly demonstrates that entrainment is strongly dependent on Re whereas the contribution from the Fr effect is relatively much smaller. The DNS results also show that z_m, which is the maximum fountain penetration height, fluctuates, even when the flow reaches full development, due to the entrainment at the upflow–downflow and the downflow–ambient interfaces, and the averaged z_m scales with $Fr^{\frac{3}{2}}Re^{\frac{1}{4}}$ for $1 < Fr \leqslant 8$ and $100 \leqslant Re \leqslant 800$.

1. Introduction

Fountain flows are common both in nature and in industrial and environmental settings. They are jet flows with a buoyancy force acting in the direction opposite to the jet direction. When a dense fluid is steadily injected upward into a miscible lighter ambient fluid, or a light fluid is directed downwards into a miscible dense ambient fluid, a fountain flow occurs.

In a quiescent homogeneous ambient fluid, the fountain behavior is predominantly governed by the Reynolds number Re, Froude number Fr, and Prandtl number Pr, defined as

$$Re = \frac{V_0 R_0}{\nu}, \quad Fr = \frac{V_0}{[R_0 g(\rho_0 - \rho_a)/\rho_a]^{1/2}}, \quad Pr = \frac{\nu}{\kappa}, \tag{1}$$

where R_0 is the nozzle radius at the fountain discharge source, V_0 is the mean discharge velocity at the source, g is the acceleration due to gravity, ρ_0 and ρ_a are the densities of jet fluid and ambient fluid at the source, and ν and κ are the kinematic viscosity and thermal diffusivity of fluid, respectively.

If the role played by the discharge momentum flux is much more important than that by the negative buoyancy flux (i.e., when $Re > 1000$ and $Fr \gg 1$), the fountain flow will become turbulent quite close to the discharge source. For such a turbulent fountain, after its initiation, the first pulse of fluid looks rather like a light starting plume, with a vortex-like front and nearly steady plume behind, as shown by the experiments conducted by Turner [1]. The velocity of the rising denser fluid is reduced gradually by the negative buoyancy until the front of this first pulse of fluid comes to rest at a temporary maximum fountain height (called the initial fountain height). After that, the flow collapses and falls back as an annular plunging plume around the upward flow. The downflow continues to mix with the ambient while also interacting turbulently with the upflow, which restricts the rise of further fluid and therefore reduces the initial height to a smaller final fountain height, and then the flow becomes steady. This final height is customarily defined as the maximum fountain penetration height. The experiments also show that the maximum fountain penetration height at full development is not constant, but fluctuates slightly and randomly.

The flow behavior of a turbulent fountain has been widely explored since the pioneering study of Morton [2,3]. One predominant parameter characterizing the flow behavior of a fountain is the maximum fountain penetration height, Z_m, and dimensional consistency requires [1]

$$z_m = \frac{Z_m}{R_0} = CFr, \tag{2}$$

where z_m is the dimensionless form of Z_m and C is a constant of proportionality. This scaling was confirmed by the experiments of Turner [1], who discharged salt jets into fresh water to produce a set of turbulent fountain flows with $0.5 < Fr < 12$ and obtained $C = 2.46$ for the final height. Many subsequent studies on turbulent

* Corresponding author. Address: School of Engineering, James Cook University, Townsville, QLD 4811, Australia. Tel.: +61 7 4781 5091; fax: +61 7 4781 6788.
E-mail address: wenxian.lin@jcu.edu.au (W. Lin).

0017-9310/$ - see front matter © 2008 Elsevier Ltd. All rights reserved.
doi:10.1016/j.ijheatmasstransfer.2008.02.047

Nomenclature

C, C_1, C_2, C_3	constants of proportionality
Fr	Froude number
g	acceleration due to gravity
H	dimensionless height of computational domain
L	dimensionless width of computational domain
n	constant defined in Eq. (3)
p	dimensionless pressure
Pr	Prandtl number
r	dimensionless radial coordinate
r_u	dimensionless upflow width
r_w	dimensionless fountain width
R_0	nozzle radius at fountain source
Re	Reynolds number
t	time
T_a	ambient fluid temperature
T_0	jet fluid temperature at fountain source
u	dimensionless radial velocity
v	dimensionless axial velocity
V_0	jet fluid vertical velocity at fountain source
z	dimensionless axial coordinate
z_m	dimensionless maximum fountain penetration height
$\bar{z}_m$	time-averaged value of z_m at full development
$z_{m,i}$	dimensionless initial maximum fountain penetration height
Z_m	maximum fountain penetration height
Greeks	
θ	dimensionless temperature
κ	thermal diffusivity
ν	kinematic viscosity
ρ_a	ambient fluid density
ρ_0	jet fluid density at fountain source
$\bar{\sigma}$	mean standard deviation
$\sigma(\bar{z}_m)$	standard deviation of $\bar{z}_m$
τ	dimensionless time
τ_i	dimensionless time for fountain to attain $z_{m,i}$

fountains have also confirmed this scaling, although a range of C values have been obtained for a wide range of Fr and Re values, as summarized in, for example, List [4], Turner [5], Gebhart et al. [6], Baines et al. [7], and more recently, Bloomfield and Kerr [8], Friedman and Katz [9], Jirka [10], and Kaye and Hunt [11].

On the other hand, if the discharge momentum flux of a fountain flow plays the same or less important role than the negative buoyancy flux, the flow will be in the laminar region. For these weak fountains with small Fr values at the order of unity, it has been shown that their flow behavior is considerably different from that of turbulent fountains. For example, it has been shown that Z_m is of the same order as R_0 for weak fountains while for turbulent fountains, as shown above, Z_m is much larger than R_0; there are no distinguishable upward and downward flows in weak fountains, instead, the streamlines curve and spread from the fountain sources, while in turbulent fountains, the upward and downward flows are clearly distinguished; there is usually little entrainment of the ambient fluid into the fountain fluid in weak fountains while such an entrainment is one of the major activities occurring in turbulent fountains; the Reynolds number affects the penetration height in laminar fountains whereas in turbulent fountains it does not. Furthermore, the experimental results of Zhang and Baddour [12] demonstrate that for $Fr < 7$, the linear Fr scaling (2) does not apply. Instead, the more appropriate scaling is found to be $z_m = C_1 Fr^{1.3}$, where C_1 is a constant of proportionality. With the assumption that in addition to the momentum flux and buoyancy flux the fluid viscosity also has an important affect on z_m, Lin and Armfield [13] showed that for weak fountains dimensional consistency requires

$$z_m = C_2 Fr Re^n, \tag{3}$$

where n is a constant which is found to be dependent on Fr and Re and C_2 is a constant of proportionality. For $Fr \sim 1$ (where the symbol "$\sim$" denotes "at the order of magnitude of") and $Re \leqslant 500$, a scaling analysis undertaken by Lin and Armfield [13] showed that $n = -1/2$, which was validated by direct numerical simulation results with $0.2 \leqslant Fr \leqslant 1$, $5 \leqslant Re \leqslant 500$, and $0.7 \leqslant Pr \leqslant 10$ [13,14]. For very weak fountains with $Fr \ll 1$, Lin and Armfield [15] argued that the inertia effect is very small and the fountain flow behavior is predominantly controlled by the buoyancy flux and the fluid viscosity and it was shown that dimensional consistency requires

$$z_m = C_3 \left(\frac{Fr}{Re}\right)^{2/3}, \tag{4}$$

where C_3 is a constant of proportionality. This scaling was validated by direct numerical simulation results with $0.0025 \leqslant Fr \leqslant 0.2$ and $5 \leqslant Re \leqslant 500$ [15].

Recently, Philippe et al. [16] carried out an experimental and theoretical study on the evolution of laminar axisymmetric fountains with $Re < 100$ and a wide range of Fr (typically $Fr \approx 10$) in miscible homogeneous fluids. By using the generalized Bernoulli theorem and based on two assumptions about the velocity profile in the jet and the ratio of the characteristic width of the whole flow with respect to the jet width, they derived an analytical solution for z_m, which, at steady state, has the following scaling relation with Fr and Re

$$z_m \simeq 0.348 Fr Re^{1/2}. \tag{5}$$

This is different from the scaling obtained by Lin and Armfield [13] which shows that $z_m \sim Fr Re^{-1/2}$. The reason for this difference is apparently due to the different ranges of Fr and Re used for the two studies. The results obtained by Lin and Armfield [13] are for weak fountains with larger Re ($5 \leqslant Re \leqslant 800$) but a small and fixed Fr ($Fr = 1$) whereas those obtained by Philippe et al. [16] are for weak fountains with much smaller Re ($0 < Re < 80$) but quite large Fr in a wide range ($1 \lesssim Fr \lesssim 200$). This is also true for other ranges of Fr and Re, as demonstrated recently by Kaye and Hunt [11], who obtained analytical solutions for $z_{m,i}$, the initial fountain penetration height, for both small and large Fr values based on a plume entrainment model. For large Fr fountains ($Fr \gtrsim 3$), they obtained $z_{m,i} \approx 2.46 Fr$, which agrees with the scaling (2); for small Fr fountains ($1 \lesssim Fr \lesssim 3$), they obtained $z_{m,i} \approx 0.90 Fr^2$; and for very small Fr fountains ($0 < Fr \lesssim 1$), they obtained $z_{m,i} \approx 0.94 Fr^{2/3}$, which is in agreement with the scaling (4) obtained by Lin and Armfield [15]. Nevertheless, all these different scaling relations obtained by different researchers reveal that the flow behavior of fountains, especially the onset of entrainment in transitional fountains with intermediate Fr and Re values ($1 \lesssim Fr \lesssim 20$, $200 \lesssim Re \lesssim 1000$), which is the key to shed light on the turbulence generation mechanism in fountains, is not well described, which motivates us to carry out this study.

In this study, we investigate the transient behavior of unsteady axisymmetric fountains in quiescent homogeneous ambient fluids with intermediate Fr and Re values ($1 \leqslant Fr \leqslant 8$ and $200 \leqslant Re \leqslant 800$; but in the $Fr = 1$ case, the upper limit of Re is extended to 2000) by direct numerical simulation (DNS). The outline of the paper is as follows. In Section 2, the physical system under consideration, governing equations, numerical methods and computational grids used in the DNS are briefly described. In Section 3, the DNS results for different sets of fountains are presented and discussed. And finally the conclusions are drawn in Section 4.

2. Governing equations and numerical methods

The physical system under consideration is a vertical circular container containing a Newtonian fluid initially at rest and at a uniform temperature of T_a, the sidewall is non-slip and insulated and the top is open. On the bottom center, an orifice with radius R_0 is used as the fountain discharge source. The remaining bottom region is a rigid non-slip and insulated boundary. At time $t = 0$, a stream of fluid at T_0 ($T_0 < T_a$) is injected upward into the container from the source to initiate the fountain flow and this discharge is maintained thereafter. The symmetry of the system geometry and the low Re values considered ensure that the flow can be assumed to be axisymmetric.

The flow is described by the following Navier–Stokes and temperature equations, which are written in non-dimensional form in cylindrical coordinates with the Boussinesq assumption as:

$$\frac{1}{r}\frac{\partial}{\partial r}(ru) + \frac{\partial v}{\partial z} = 0, \tag{6}$$

$$\frac{\partial u}{\partial \tau} + \frac{1}{r}\frac{\partial}{\partial r}(ruu) + \frac{\partial}{\partial z}(vu) = -\frac{\partial p}{\partial r} + \frac{1}{Re}\left\{\frac{\partial}{\partial r}\left[\frac{1}{r}\frac{\partial}{\partial r}(ru)\right] + \frac{\partial^2 u}{\partial z^2}\right\}, \tag{7}$$

$$\frac{\partial v}{\partial \tau} + \frac{1}{r}\frac{\partial}{\partial r}(ruv) + \frac{\partial}{\partial z}(vv) = -\frac{\partial p}{\partial z} + \frac{1}{Re}\left[\frac{1}{r}\frac{\partial}{\partial r}\left(r\frac{\partial v}{\partial r}\right) + \frac{\partial^2 v}{\partial z^2}\right] + \frac{1}{Fr^2}\theta, \tag{8}$$

$$\frac{\partial \theta}{\partial \tau} + \frac{1}{r}\frac{\partial}{\partial r}(ru\theta) + \frac{\partial}{\partial z}(v\theta) = \frac{1}{RePr}\left[\frac{1}{r}\frac{\partial}{\partial r}\left(r\frac{\partial \theta}{\partial r}\right) + \frac{\partial^2 \theta}{\partial z^2}\right], \tag{9}$$

where all lengths, velocities, times, pressures, and temperatures are made dimensionless by R_0, V_0, R_0/V_0, $\rho_0 V_0^2$, $(T_0 - T_a)$, respectively.

The governing equations are discretized on a non-staggered mesh using finite volumes, with standard second-order central difference schemes used for the viscous, pressure gradient and divergence terms. The QUICK third-order upwind scheme is used for the advective terms. The second-order Adams-Bashforth scheme and Crank-Nicolson scheme are used for the time integration of the advective terms and the diffusive terms, respectively. To enforce the continuity, the pressure correction method is used to construct a Poisson's equation which is solved using the preconditioned GMRES method. Detailed descriptions of these schemes were given in [17], and the code has been widely used for the direct simulation of a range of buoyancy dominated flows, including the travelling waves in natural convection in a cavity [18], weak fountain flows [13–15,19], and unsteady natural convection flows [20–22].

To ensure that suitable resolutions are maintained in the numerical simulations, non-uniform computational meshes have been used which concentrate points in the regions near the boundaries and with high gradients of temperature and velocities and are relatively coarse in the remaining regions. The constructed meshes have 296×299 grid points for the $Fr = 1$ simulations, 298×297 grid points for the $Fr = 2$, 4 and 6 simulations, and 298×299 grid points for the $Fr = 8$ simulations. The time steps of 10^{-4} and 2.5×10^{-4} are used for the $Fr = 1$ and 2 simulations, whereas 5×10^{-5} is used for the $Fr = 4$, 6 and 8 simulations, respectively, where the time steps are made dimensionless by R_0/V_0. An extensive mesh and time-step dependency analysis has been carried out to ensure that the solutions are accurate with minimal grid and time-step dependent error.

3. DNS results and discussions

To show the effects of Fr and Re on the onset of entrainment in fountain flows, four sets of DNS of axisymmetric fountains in quiescent homogeneous fluids with selected values of Fr and Re have been carried out. The selected values of Fr, Re and $L \times H$ used for these cases are listed in Table 1, where L and H are the dimensionless width and height of the computational domain which is one half of the physical domain (L and H are made dimensionless by R_0). The $Fr = 1$, 2 and 6 fountains have been chosen to show the effect of Re on small, medium, and large Fr fountains, respectively, whereas the $Fr = 4$ and 8 fountains have been chosen to give further results. As the effect of Pr is not included in this study, a fixed $Pr = 7$ has been used in all DNS.

The predominant parameters characterizing the transient fountain behavior are the dimensionless maximum fountain penetration height z_m as defined above, the upflow width r_u, and the fountain width r_w. The parameters r_u and r_w, both made dimensionless by R_0, denote, respectively, the location of the upflow–downflow interface at which the vertical velocity of the fluid becomes zero, and the location of the downflow–ambient interface where the fluid temperature is 1% of the temperature difference between the jet fluid and the ambient fluid at the source. The definitions of these parameters are given in Fig. 1, where typical vertical profiles of r_u and r_w at full development are presented for the specific cases of $Fr = 6$ at $Re = 200$ and 600, respectively.

3.1. Temperature contours

To illustrate the transient flow behavior of the small, medium, and large Fr fountains, Figs. 2–4 present the evolution of temperature contours for the $Fr = 1$ fountains, 2 fountains and 6 fountains, respectively.

From the left column of Fig. 2, which presents the snapshots of temperature contours at $\tau = 1$, 5, 10, 20 and 40 for the $Fr = 1$ fountains at $Re = 500$, it is evident that during the whole evolution of the fountain, there is essentially no entrainment between the jet fluid and the ambient fluid. This is true for the $Fr = 1$ fountains at a Reynolds number as high as 1000, as demonstrated in the right column of Fig. 2, which presents the snapshots of temperature contours at $\tau = 40$ for the $Fr = 1$ fountains at $Re = 200$, 500, 1000, 1200 and 2000, respectively. However, the figure also shows that when

Table 1
The selected values of Fr and Re and $L \times H$ used in the four sets of DNS of axisymmetric fountains

DNS set	Fr	Re	$L \times H$
$Fr = 1$ fountains	1	200	15×6
	1	500	15×6
	1	1000	15×6
	1	1200	15×6
	1	2000	15×6
$Fr = 2$ fountains	2	100	25×10
	2	200	25×10
	2	300	25×10
	2	500	25×10
	2	800	25×10
$Fr = 4$ fountains	4	200	60×40
	4	500	60×40
$Fr = 6$ fountains	6	100	60×40
	6	200	60×40
	6	300	60×40
	6	500	60×40
	6	800	60×40
$Fr = 8$ fountains	8	200	60×60
	8	500	60×60

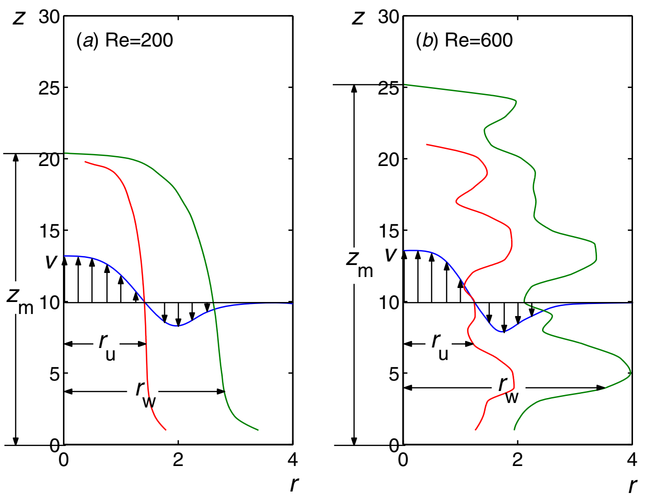

Fig. 1. Typical vertical profiles of r_u and r_w at full development for the $Fr = 6$ fountains with: (a) $Re = 200$ and (b) $Re = 600$, and the definitions of z_m, r_u, and r_w.

$Re \geqslant 1200$, entrainment is present in the fountains, although mainly at the interface between the downflow of the jet fluid and the ambient fluid.

When the Froude number increases, as illustrated in Figs. 3 and 4 for the $Fr = 2$ and 6 fountains, respectively, entrainment is present for a Reynolds number as low as 200 and the extent of entrainment is found to approximately increase with Re. Similar phenomena are also found for the $Fr = 4$ and 8 fountains, although the snapshots for these fountains are not presented to avoid repetition.

3.2. Fountain penetration height

The time series of z_m for the $Fr = 1$ fountains at $Re = 200$, 500, 1000, 1200 and 2000 are presented in Fig. 5, where it is observed that at the early stage of evolution (when $\tau < 2$), all five time series of z_m are essentially the same. In fact, it can be further observed that the three time series at $Re \geqslant 1000$ are essentially the same until $\tau \simeq 12$, at which time the upflows and downflows in the fountains are fully developed. However, the time series for $Re \leqslant 500$ begin to deviate from the higher Re ones when $\tau > 2$, and the deviation increases when Re is reduced, reaching its maximum when the fountain attains the initial maximum penetration height $z_{m,i}$. Nevertheless, the deviation is quite small as the maximum deviations presented in the time series at $Re = 200$ and 500 are only 3.4% and 1.7%, respectively, from the higher Re results and all time series reach their individual $z_{m,i}$ at almost the same time ($\tau \simeq 4$). Furthermore, if z_m and τ are scaled, respectively, by $z_{m,i}$ and τ_i, where τ_i is the time to attain $z_{m,i}$, it is seen, from Fig. 5b, that for $\tau \leqslant \tau_i$ all five scaled time series collapse onto a single curve. On the other hand, when the fountains attain full development (when $\tau > 20$), z_m for $Re \leqslant 1000$ is constant, whereas z_m for $Re > 1000$ oscil-

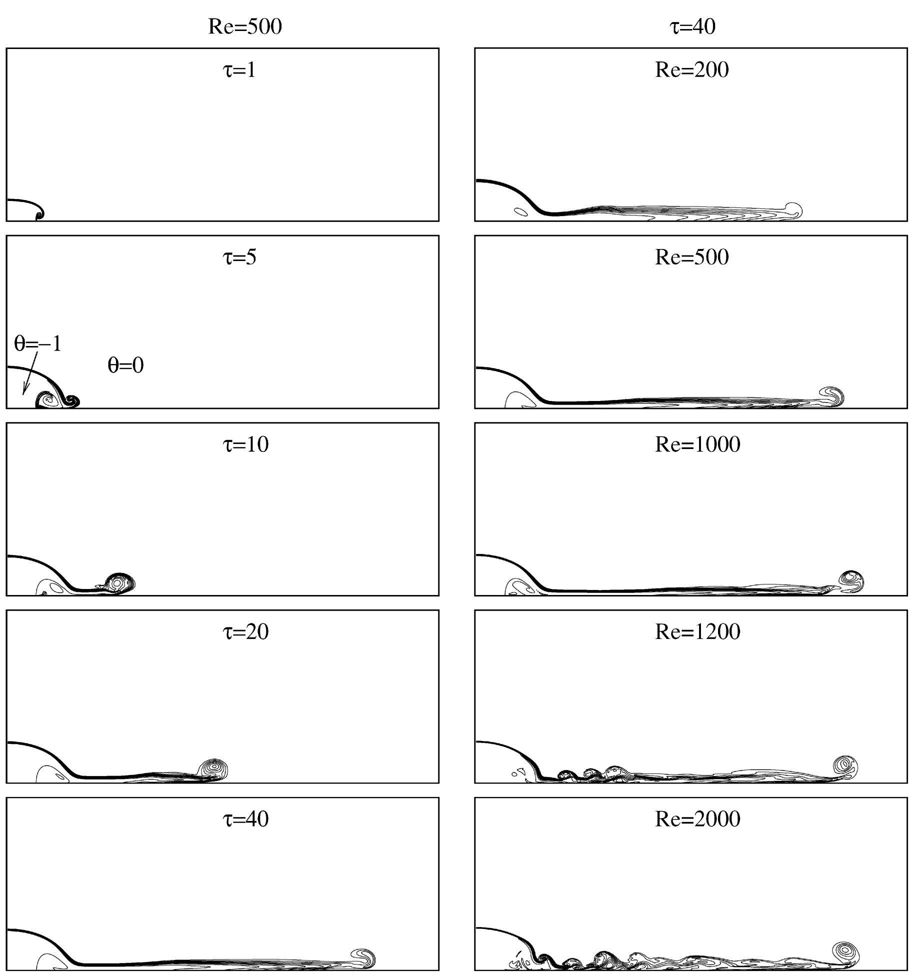

Fig. 2. Temperature contours for the $Fr = 1$ fountains. The left column is for $Re = 500$ at five specific times, and the right column is for five Reynolds numbers at $\tau = 40$.

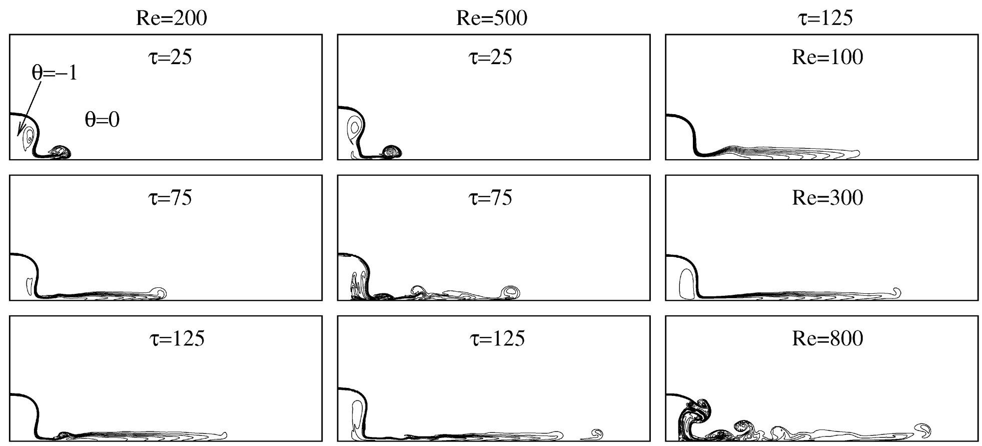

Fig. 3. Temperature contours of the $Fr = 2$ fountains with $Re = 200$ (left column) and 500 (middle column) at $\tau = 25$, 75 and 125, and with $Re = 100$, 300 and 800 at $\tau = 125$ (right column).

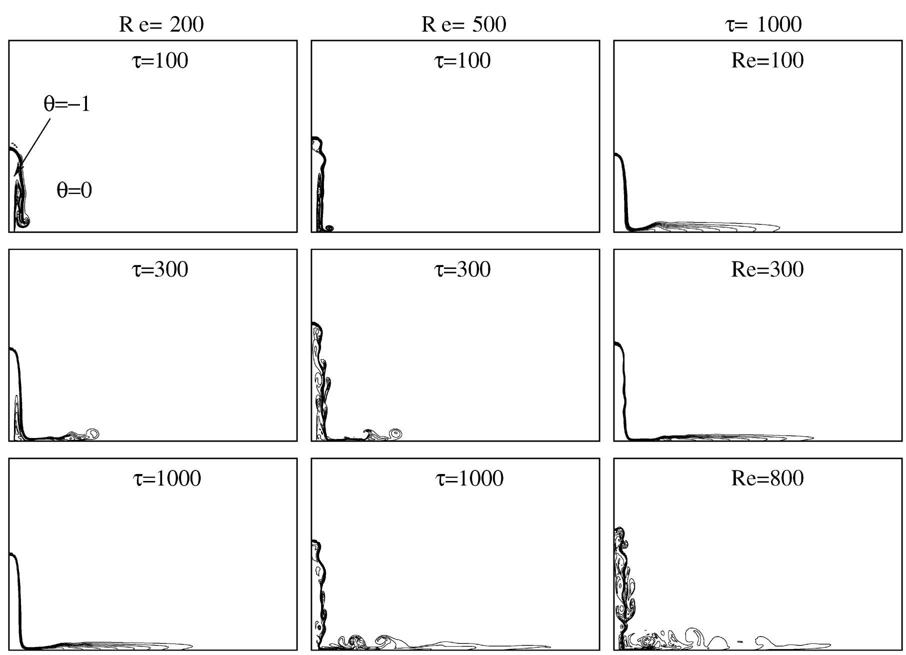

Fig. 4. Temperature contours of the $Fr = 6$ fountains (left column) and 500 (middle column) at $\tau = 100$, 300 and 1000, and with $Re = 100$, 300 and 800 at $\tau = 1000$ (right column).

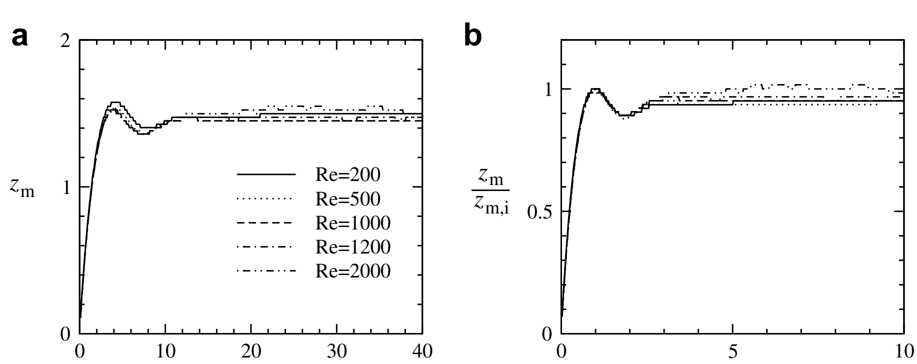

Fig. 5. Time series of z_m for the $Fr = 1$ fountains: (a) raw data and (b) z_m scaled by $z_{m,i}$ and τ scaled by τ_i.

lates, with standard deviations of 0.008 and 0.017 over $20 \leqslant \tau \leqslant 40$. Hence, the DNS results show that Re has little effect on z_m for the $Fr = 1$ fountains when $200 \leqslant Re \leqslant 2000$.

The time series of z_m of the $Fr = 2$ fountains at $Re = 100$, 200, 300, 500 and 800 are presented in Fig. 6, which shows that when $\tau \leqslant 15.8$, all five time series of z_m are essentially the same. Nevertheless, the time series with $Re = 100$ and 200 reach their individual $z_{m,i}$ at about $\tau = 35$ and 35.4, although those with $Re = 300$, 500 and 800 reach their individual $z_{m,i}$ almost at the same time (at $\tau \simeq 31$). Furthermore, it is observed that $z_{m,i}$ increases slightly with Re, from 3.592 at $Re = 100$ to 4.95 at $Re = 800$. At full development (when $\tau > 70$), z_m with $Re = 100$ and 300 oscillates a little bit, with a very small standard deviation of 0.068 and 0.038, respectively, over $75 \leqslant \tau \leqslant 150$. However, z_m with $Re \geqslant 500$ oscillates considerably, with standard deviations of 0.201 and 0.372 for $Re = 500$ and 800, respectively, over $75 \leqslant \tau \leqslant 150$. The averaged values of z_m of these $Fr = 2$ fountains at full development are 3.702, 4.094, 3.699, 4.304 and 3.926 for $Re = 100$, 200, 300, 500 and 800, respectively, indicating that Re has little effect on the averaged values of z_m of these $Fr = 2$ fountains. Nonetheless, it should also be noted that z_m of the $Fr = 2$ fountains at $Re = 200$ oscillates significantly at full development, with a large standard deviation of 0.222 over $75 \leqslant \tau \leqslant 150$, which is much larger than that at $Re = 300$, and even a little bit larger than that at $Re = 500$. It is also observed that the $Re = 200$ oscillation is regular with a periodic or quasi-periodic behavior, whereas the $Re = 500$ oscillation is irregular with a non-periodic chaotic structure. Further study of animations for $Re = 200$ and 500 suggests that separate mechanisms are responsible for the oscillatory behavior at each Re. The $Re = 200$ flow exhibits a periodic bobbing motion, whereas the $Re = 500$ flow appears to be driven by an instability in the shear layer between the fountain core and falling flow. It is therefore considered likely that the $Re = 200$ flow is driven by a narrow banded instability which, at this Re only of those considered, exhibits a single mode resonance. The instability driving the $Re = 500$ flow would appear to be broad banded with a range of unstable modes leading to the observed non-periodic, chaotic behavior. The $Re = 300$ flow is below the critical Re for the occurrence of the broad banded instability occurring at $Re = 500$, and does not produce the resonant single mode behavior observed at $Re = 200$. Hence, the DNS results show that at full development Re affects the oscillation amplitude of z_m of the $Fr = 2$ fountains when $Re \geqslant 500$, although it has little effect on the averaged value of z_m.

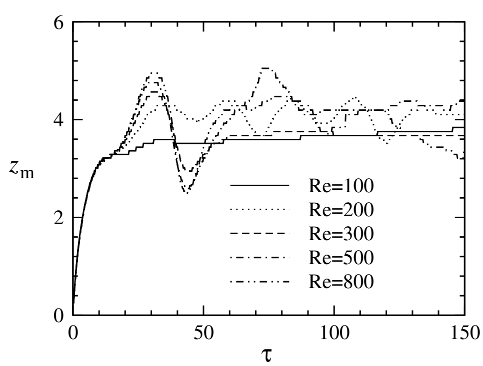

Fig. 6. Time series of z_m of the $Fr = 2$ fountains.

The time series of z_m for the $Fr = 6$ fountains at $Re = 100$, 200, 300, 500 and 800 are presented in Fig. 7, where it is observed that when $\tau \lesssim 40$, all five time series are essentially the same. However, $z_{m,i}$ and τ_i are found to increase steadily with Re, although the increase rates are not large, from $z_{m,i} = 16.03$ and $\tau_i = 69.5$ at $Re = 100$ to $z_{m,i} = 20.96$ and $\tau_i = 102.3$ at $Re = 800$, respectively. Nevertheless, if z_m and τ are scaled, respectively, by $z_{m,i}$ and τ_i, the scaled time series of these $Fr = 6$ fountains will collapse onto a single curve for $\tau \leqslant \tau_i$, as shown in Fig. 7b. The results also show that at full development there are oscillations present in the time series of z_m when $Re \geqslant 200$ and the mean value of z_m at full development increases steadily with Re, from 20.2 at $Re = 200$ to 27.2 at $Re = 800$ over $500 \leqslant \tau \leqslant 1000$. The amplitude of oscillations is also found to increase with Re, with standard deviations of 0.147, 0.854, 2.499 and 2.891 over $500 \leqslant \tau \leqslant 1000$ for $Re = 200$, 300, 500 and 800, respectively. However, there is no oscillation present in the time series of z_m at $Re = 100$ and z_m is constant ($z_m = 16.4$) from $\tau = 500$ to 1000. Hence, the DNS results show that Re has a trivial effect on z_m for $Fr = 6$ fountains only when $Re \lesssim 200$ and when $Re > 200$ its effect on z_m becomes significant and the extent of this effect increases dramatically with Re.

The DNS results also show that Re has a considerably effect on z_m when $Re \geqslant 200$ for the $Fr = 4$ and 8 fountains and the extent of effect increases dramatically with Re, similar to that for the $Fr = 2$ and 6 fountains as observed above.

3.3. Upflow and fountain widths

The Re effect on r_u and r_w of the $Fr = 1$ fountains is not trivial, as illustrated in Fig. 2, where it is found that for $Re > 1000$ entrainment is present at the interface between the downflow and the ambient fluid as well as between the horizontal intrusion, which moves outwards along the bottom floor, and the ambient fluid, with the extent increasing with Re. The entrainment and associated waves at the intrusion–ambient interface are characterized as "internal bores" and were explored in detail by Simpson [23].

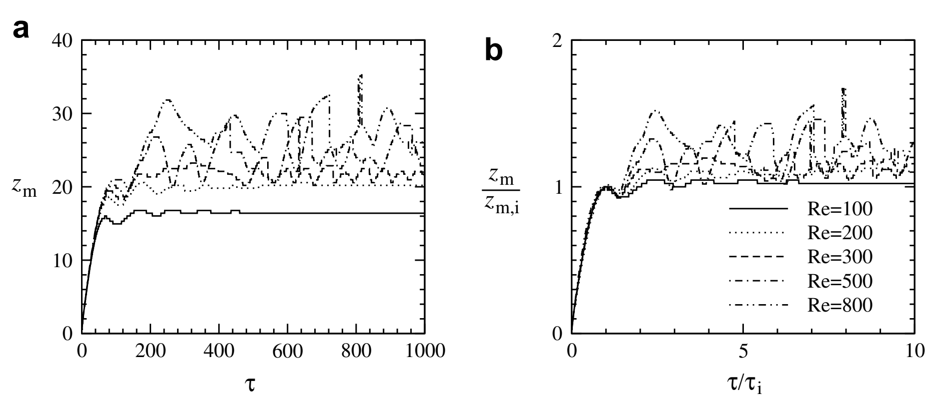

Fig. 7. Time series of z_m for the $Fr = 6$ fountains: (a) raw data and (b) z_m scaled by $z_{m,i}$ and τ scaled by τ_i.

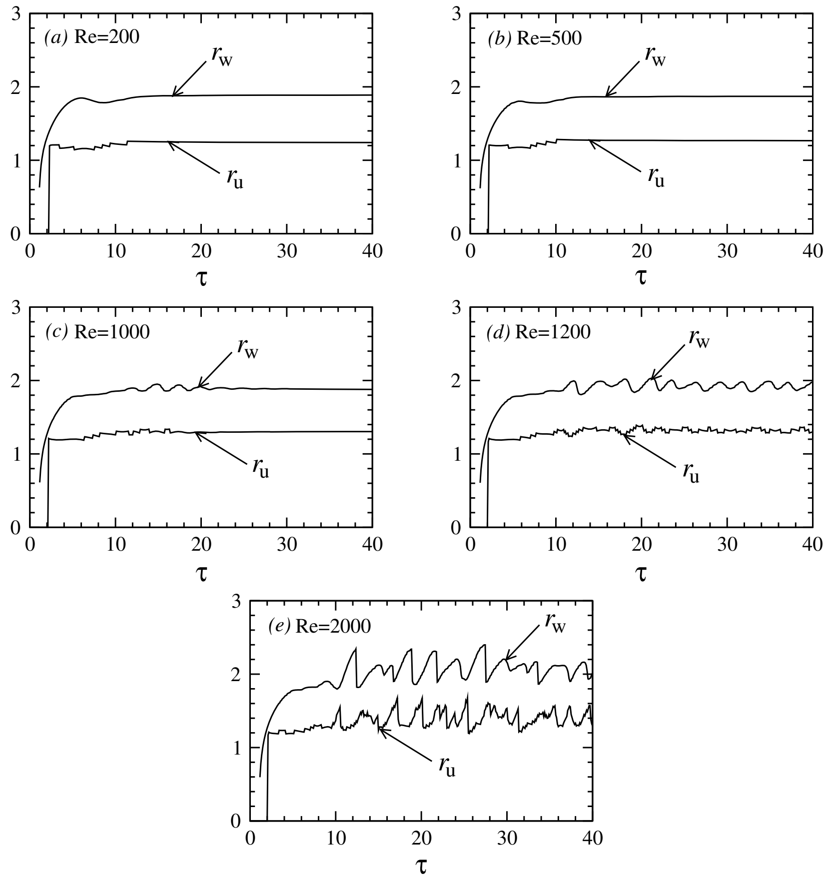

Fig. 8. Time series of r_u and r_w of the $Fr = 1$ fountains at $z = 0.8$.

The *Re* effect on r_u and r_w for these $Fr = 1$ fountains is more clearly seen in Fig. 8, where typical time series of r_u and r_w at $z = 0.8$ are presented for the five $Fr = 1$ fountains considered. The results show that non-trivial oscillations, which represent the entrainment, are present in the full development time series of both r_u and r_w when $Re > 1000$ and their amplitudes increase considerably with *Re*. Furthermore, it is also found that the entrainment becomes stronger at smaller *z*, as seen in Fig. 9 by the larger variation with respect to the time average values, where the vertical profiles of r_u and r_w of the $Fr = 1$ fountains at $\tau = 20$, 30 and 40 and their time-averaged values over $20 \leqslant \tau \leqslant 40$ are presented. When $Re \leqslant 500$, the vertical profiles of r_u and r_w at these times, as shown in Fig. 9a–d, are essentially the same, and their smooth and well-defined shapes indicate that there is no entrainment at the upflow–downflow interface and at the downflow–ambient interface. Additionally, no entrainment is found to be present at the intrusion–ambient interface for $Re \leqslant 500$. When $Re \geqslant 1000$, however, the shapes of the vertical profiles of r_u and r_w at $\tau = 20$, 30 and 40 differ from each other and become oscillatory, especially in the small *z* regions, and the differences and the oscillations increase with *Re*, as shown in Fig. 9e–j, indicating that entrainment occurs in these regions of the interfaces.

Re is also found to have a large effect on r_u and r_w for $Fr = 2$ fountains, as shown in Fig. 3, where it is clearly seen that when $Re \geqslant 500$ entrainment is present at the upflow–downflow interface, at the downflow–ambient interface and at the intrusion–ambient interface, and the extent increases with *Re*. More specifically, as shown in Fig. 10, where the time series of r_u and r_w of the $Fr = 2$ fountains with $100 \leqslant Re \leqslant 800$ at $z = 1.6$ are presented, it is shown that significant oscillations are present in the full development time series of both r_u and r_w when $Re \geqslant 500$ and the oscillation amplitudes increase considerably with *Re*, with standard deviations of 0.167 and 0.482 in r_u and 0.21 and 0.81 in r_w for $Re = 500$ and 800, respectively, from $\tau = 75$ to 150. However, the oscillation amplitudes of these $Fr = 2$ fountains at $Re = 100$ and 300 are very small, with standard deviations of 0.025 and 0.03 in r_u and 0.019 and 0.02 in r_w for $Re = 100$ and 300, respectively, over the same time period, clearly showing that essentially no entrainment is present at $Re = 100$ and 300. Nevertheless, similar to z_m, it is also seen that large oscillations are present in r_u and r_w at $Re = 200$, as shown in Fig. 10, with standard deviations of 0.119 in r_u and 0.161 in r_w over $75 \leqslant \tau \leqslant 150$, indicating that non-trivial entrainment is present in this $Fr = 2$ fountains at $Re = 200$, due to the same mechanisms described above.

The above observation of the *Re* effects on r_u and r_w of the $Fr = 2$ fountains are found to be true at other heights as well. In fact, the results shown in Fig. 11, where the vertical profiles of r_u and r_w of the five $Fr = 2$ fountains at $\tau = 100$, 125 and 150 as well as their averaged values over $75 \leqslant \tau \leqslant 150$ are presented, show that all profiles presented in each of Fig. 11a, b, e and f for $Re = 100$ and 300, are essentially the same, meaning that the *Re* effect is negligible at these *Re*. The smooth and well-defined shapes of these profiles and the temperature contours presented in Fig. 3 also indicate that there is no entrainment present in these fountains. However, when $Re \geqslant 500$, as shown in Fig. 11g–j, the profiles at the three specific times differ from each other and oscillations are present in the profiles, with the extent of the differences and oscillations increasing significantly with *Re*, suggesting that large entrainment is present at the upflow–downflow interface, at the downflow–ambient interface, at the intru-

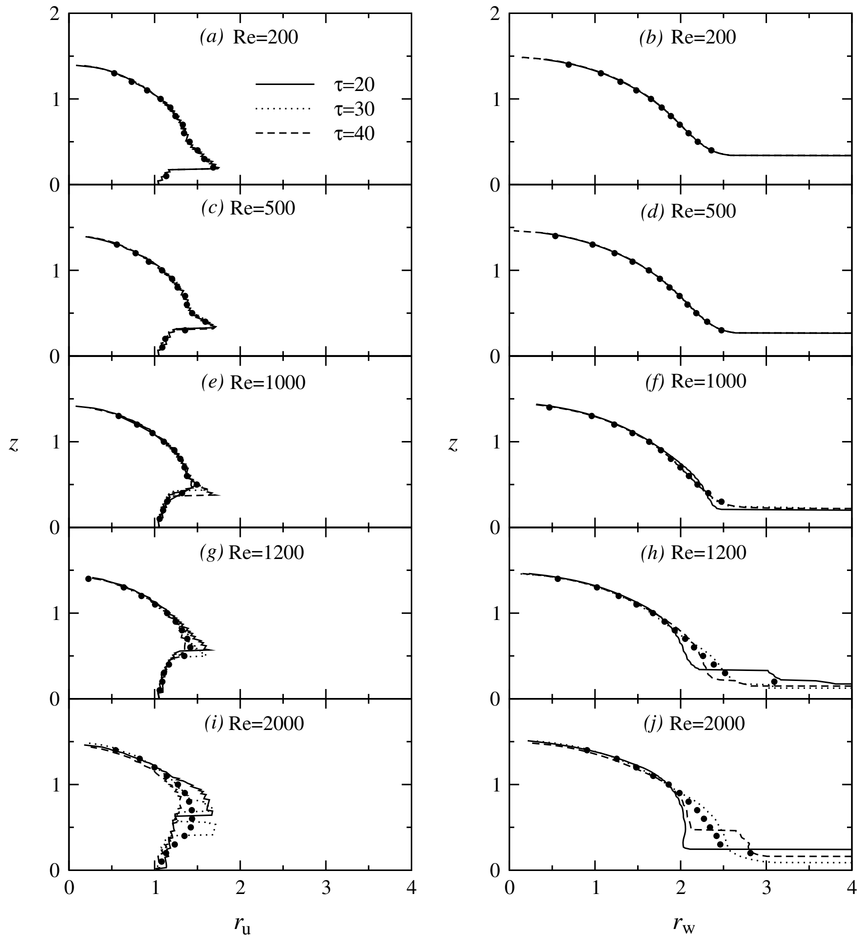

Fig. 9. Vertical profiles of r_u (left column) and r_w (right column) of the $Fr = 1$ fountains at $\tau = 20$, 30 and 40. The symbol "●" denotes the time-averaged value over $20 \leqslant \tau \leqslant 40$.

sion–downflow interface, and occasionally even at the upflow–ambient interface when the upflow penetrates the downflow and directly entrains the ambient fluid.

Similar *Re* effects are also found on r_u and r_w for the $Fr = 6$ fountains, as shown as an example in Fig. 12, where the typical time series of r_u and r_w at $z = 10$ are presented for the five $Fr = 6$ fountains. The results show that at this specific height, when $Re \leqslant 200$, r_u and r_w at full development (i.e. when $\tau \gtrsim 300$) are constant, with $r_u = 1.411$ at both $Re = 100$ and 200 and $r_w = 2.764$ and 2.595 at $Re = 100$ and 200, respectively, indicating that *Re* has a negligible effect on r_u and r_w when $Re \leqslant 200$. Furthermore, as there is no oscillation present in the full development time series of r_u and r_w when $Re \leqslant 200$, there is no entrainment at the interfaces of the upflow–downflow, the downflow–ambient, and the intrusion–ambient, which is also clearly shown in Fig. 4. Hence, even for *Fr* as large as 6, there is no entrainment in the fountains when $Re \leqslant 200$. Nevertheless, oscillations are present in the full development time series of both r_u and r_w when $Re \geqslant 300$, and their amplitudes are found to increase substantially with *Re*, with standard deviations of 0.093, 0.245 and 0.387 in r_u and 0.078, 0.313 and 0.961 in r_w over $500 \leqslant \tau \leqslant 1000$ when $Re = 300$, 500 and 800, respectively. Entrainment occurs at the interfaces of the upflow–downflow, the downflow–ambient, and the intrusion–ambient, and the extent increases with *Re*, as evident in Figs. 4 and 12. In the case of $Re = 800$, it is further seen from Fig. 12i and j that at some instants r_u is even larger than r_w, indicating that the upflow penetrates the downflow and directly entrains the ambient fluid. It is expected that this upflow–ambient entrainment will become stronger when *Re* is further increased.

The above observations are also found to be true at other heights as well. Fig. 13 presents vertical profiles of r_u and r_w of the five $Fr = 6$ fountains at $\tau = 500$, 750 and 1000 as well as their averaged values over $500 \leqslant \tau \leqslant 1000$. It is seen that all profiles presented in each of Fig. 13a–d, where $Re \leqslant 200$, are essentially the same, meaning that the *Re* effect is negligible when $Re \leqslant 200$. The smooth and well-defined shapes of these profiles and the temperature contours presented in Fig. 4 also suggest that there is no entrainment present in these low *Re* fountains, even at *Fr* as high as 6. However, when $Re \geqslant 300$, as shown in Fig. 13e–j, the profiles at the three specific times differ from each other and the differences are found to increase significantly with *Re*. The oscillatory shapes of these profiles and the temperature contours presented in Fig. 4 mean that entrainment is present at the upflow–downflow interface, at the downflow–ambient interface, at the intrusion–downflow interface, and even at the upflow–ambient interface at some instants.

The DNS results also show that all above-mentioned observations on r_u and r_w obtained for the $Fr = 2$ and 6 fountains are true for the $Fr = 4$ and 8 fountains. Hence, it can be concluded that for $Fr \geqslant 2$ fountains *Re* has a little effect and there is little entrainment in the flow even when *Fr* is as high as 8 when $Re \leqslant 200$, but its effect and the entrainment become substantial when $Re \geqslant 200$, as considerable entrainment is present at the upflow–downflow interface, at the downflow–ambient interface, at the intrusion–downflow interface, and even at the upflow–ambient interface at some instants.

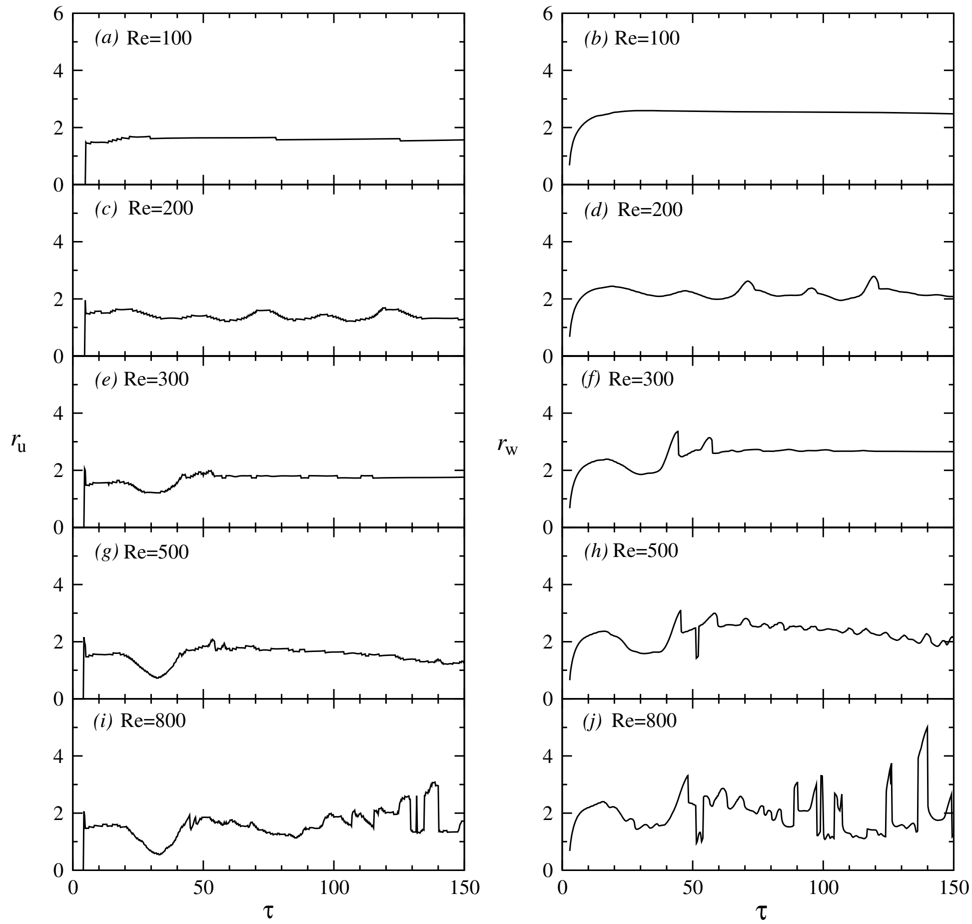

Fig. 10. Time series of r_u (left column) and r_w (right column) of the $Fr = 2$ fountains at $z = 1.6$.

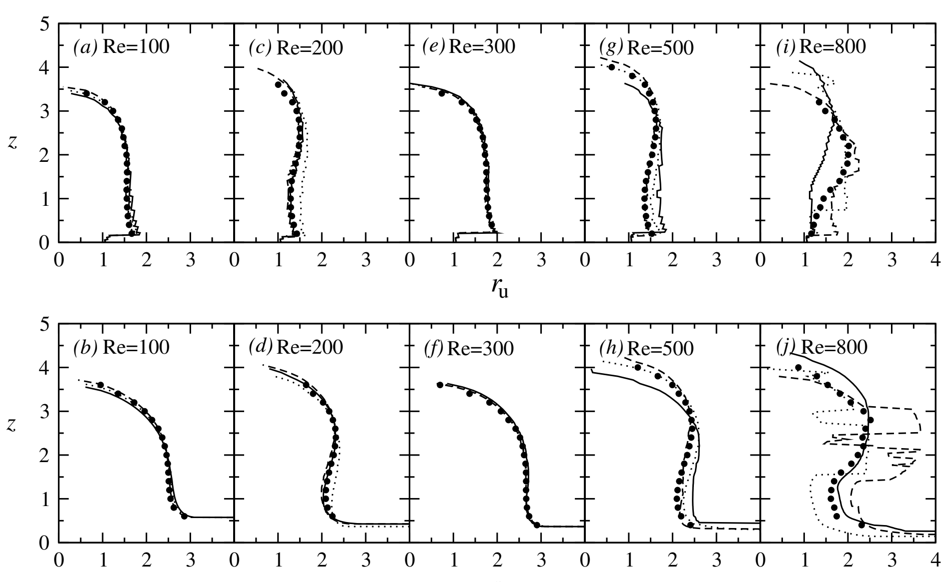

Fig. 11. Vertical profiles of r_u (upper row) and r_w (bottom row) of the $Fr = 2$ fountains at $\tau = 100$ (—), 125 (···), and 150 (– – –). The symbol "•" denotes the time-averaged values over $100 \leqslant \tau \leqslant 150$.

3.4. Steady state and fluctuations

At full development, the entrainment at the upflow–downflow interface and at the downflow–ambient interface at a specific height z are well quantified by the respective standard deviations in the full development time series of r_u and r_w at z over a period of time. The mean standard deviations $\overline{\sigma}$ of r_u and r_w for all the fountains considered here are presented in Fig. 14. For the $Fr = 1$,

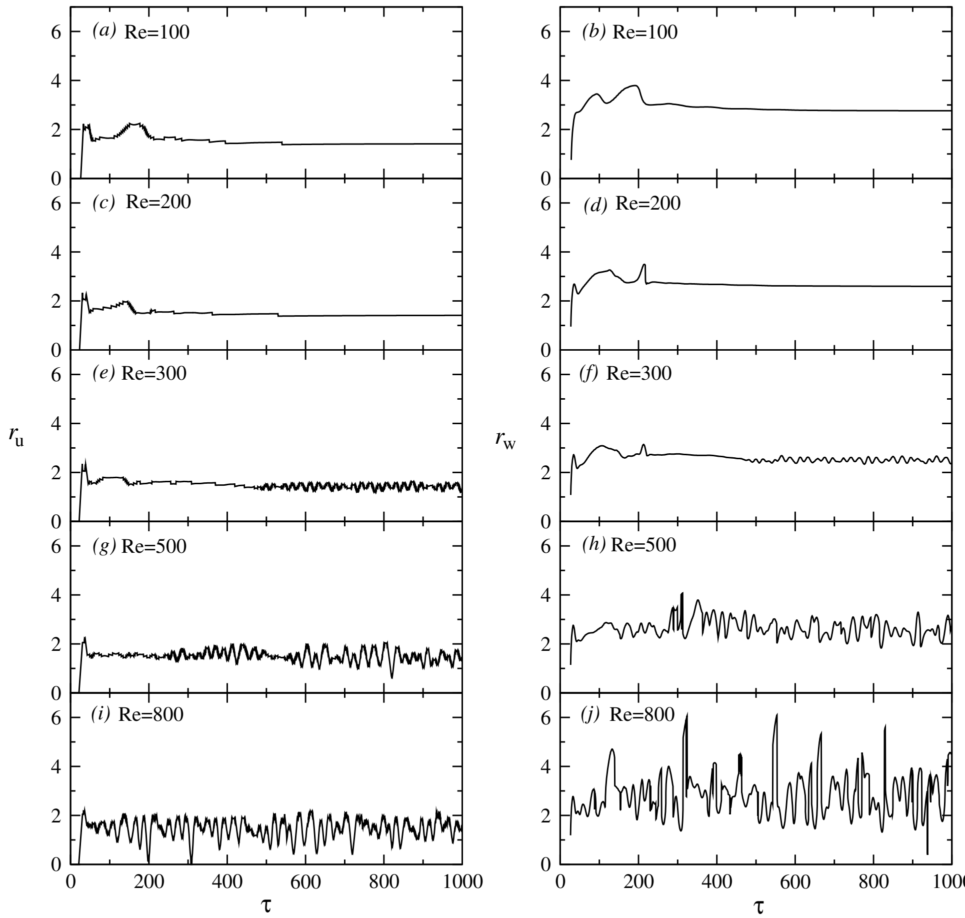

Fig. 12. Time series of r_u (left column) and r_w (right column) of the $Fr = 6$ fountains at $z = 10$.

2, 4 and 8 fountains, the averages are obtained over $0.4 \leqslant z \leqslant 1.2$ from $\tau = 20$ to 40, $0.6 \leqslant z \leqslant 3.2$ from $\tau = 100$ to 150, $2 \leqslant z \leqslant 10$ from $\tau = 300$ to 800, and $3 \leqslant z \leqslant 28$ from $\tau = 750$ to 1150, respectively. For the $Fr = 6$ fountains, the averages are obtained over $3 \leqslant z \leqslant 15$ (for $Re = 100$), $3 \leqslant z \leqslant 18$ (for $Re = 200$ and 300), $3 \leqslant z \leqslant 20$ (for $Re = 500$), and $4 \leqslant z \leqslant 25$ (for $Re = 800$), all from $\tau = 500$ to 1000.

From this figure, it is clearly seen that for the $Fr = 1$ fountains, when $Re \leqslant 500$, the mean standard deviations are very small ($\overline{\sigma} < 0.002$) and are essentially independent of *Re*, indicating that there is essentially no entrainment present at the interfaces, which is in agreement with the above observations. However, when $Re \geqslant 1000$, the mean standard deviations of both r_u and r_w are not trivial and increase substantially with *Re*. The data are best fitted by the following power-laws:

$$\overline{\sigma} = 4.08 \times 10^{-7} Re^{1.60}, \tag{10}$$

for r_u and

$$\overline{\sigma} = 8.23 \times 10^{-9} Re^{2.14}, \tag{11}$$

for r_w, respectively, which clearly show that entrainment is present at both the upflow–downflow interface and the downflow–ambient interface, and their extent increases with *Re*, which is again in agreement with the above observations.

For the $Fr = 2$ fountains, the results show that when $Re = 100$ and 300 the mean standard deviations are negligible with $\overline{\sigma} < 0.036$, indicating that there is essentially no entrainment present at the interfaces, which is in agreement with the above observations. However, when $Re \geqslant 500$, the mean standard deviations of both r_u and r_w are large, with $\overline{\sigma} = 0.116$ and 0.363 in r_u and $\overline{\sigma} = 0.136$ and 0.74 in r_w for $Re = 500$ and 800, respectively. Therefore, the mean standard deviations in both r_u and r_w of these $Fr = 2$ fountains at $Re \geqslant 500$ increase considerably with *Re*, clearly showing that entrainment is present at the upflow–downflow interface and at the downflow–ambient interface and their extent increases dramatically with *Re*, which is again in agreement with the above observations. However, similar to the above-observed large value of the mean standard deviation of z_m when $Re = 200$, large standard deviations of 0.098 and 0.136 are found in r_u and r_w, respectively, over $0.6 \leqslant z \leqslant 3.2$ and over $100 \leqslant \tau \leqslant 150$ for the $Fr = 2$ fountains at $Re = 200$. Similar observations on the mean standard deviations $\overline{\sigma}$ of r_u and r_w are also found for higher Froude number fountains. As shown in the figure, for all $Fr \geqslant 2$ fountains considered, the DNS results show that the mean standard deviations of both r_u and r_w are best fitted by the following power-laws:

$$\overline{\sigma} = 3.39 \times 10^{-5} Re^{1.38}, \tag{12}$$

for r_u and

$$\overline{\sigma} = 3.72 \times 10^{-6} Re^{1.79}, \tag{13}$$

for r_w, respectively, which clearly show that entrainment is present at both the upflow–downflow interface and the downflow–ambient interface, and their extent increases with *Re*, which is again in agreement with the above observations.

Fig. 15 presents $\overline{z}_m$, which is plotted against $Fr^{3/2}Re^{1/4}$, and $\sigma(\overline{z}_m)$, which is plotted against *Re*, for all *Fr* and *Re* considered, where $\overline{z}_m$ is the time-averaged value of z_m at full development and $\sigma(\overline{z}_m)$ is its

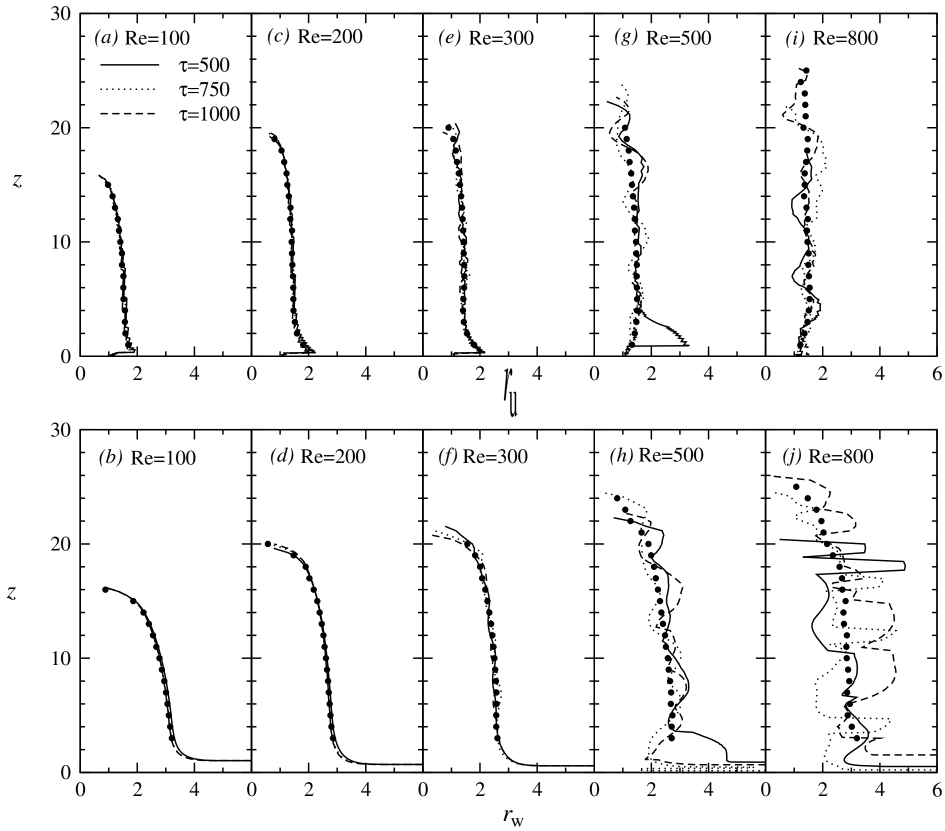

Fig. 13. Vertical profiles of r_u (upper row) and r_w (bottom row) of the $Fr = 6$ fountains at $\tau = 500$, 750 and 1000. The symbol "●" denotes the time-averaged values over $500 \leqslant \tau \leqslant 1000$.

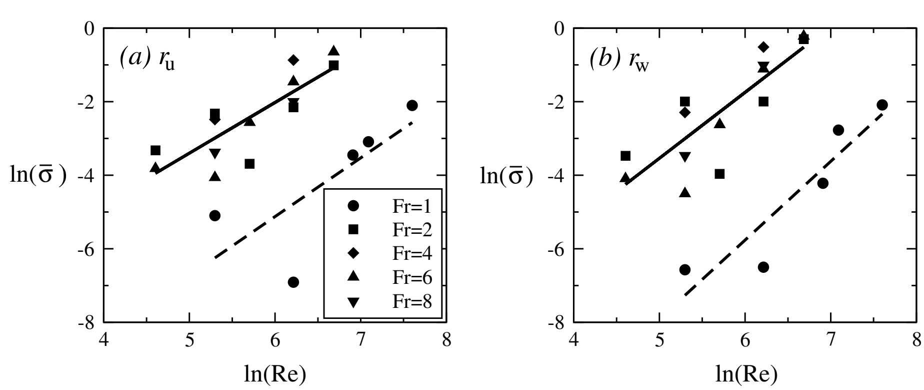

Fig. 14. Mean standard deviations of r_u (a) and r_w (b) plotted against Re for all fountains considered: (a) $\bar{\sigma} = 4.08 \times 10^{-7} Re^{1.60}$ (– – –), fit-curve for the $Fr = 1$ fountains considered, $\bar{\sigma} = 3.39 \times 10^{-5} Re^{1.38}$ (—), fit-curve for the $Fr \geqslant 2$ fountains considered and (b) $\bar{\sigma} = 8.23 \times 10^{-9} Re^{2.14}$ (– – –), fit-curve for the $Fr = 1$ fountains considered, $\bar{\sigma} = 3.72 \times 10^{-6} Re^{1.79}$ (—), fit-curve for the $Fr \geqslant 2$ fountains considered.

standard deviation. It is seen that the DNS results show that $\bar{z}_m$ can be approximated by the following empirical relation:

$$\bar{z}_m = 0.359 Fr^{3/2} Re^{1/4}, \tag{14}$$

and $\sigma(\bar{z}_m)$ increases monotonically with Re when $Fr > 2$, which can be approximated by the following empirical relation:

$$\sigma(\bar{z}_m) = 9.17 \times 10^{-6} Re^2. \tag{15}$$

The scaling relation obtained here shows that the fountain height is dependent on both Fr and Re, as has been observed previously. However the specific power-law relations have not been obtained previously. It is noted that the Fr and Re values used in this study were chosen to give flows in the transition regime, whereas most previous studies considered either fully turbulent or steady laminar flows. The Re dependency in particular is seen to vary significantly. Lin and Armfield [15] reported an inverse relationship between fountain height and Re for very weak fountains with $Re < 500$, while for strong, fully turbulent fountains no Re dependency is observed. It may be hypothesized that in the case considered here the increase in entrainment associated with an increase in Re leads to reduced negative buoyancy in the downflowing fluid, mitigating the effect of the downflowing fluid constraining the upward flowing fluid in the fountain core.

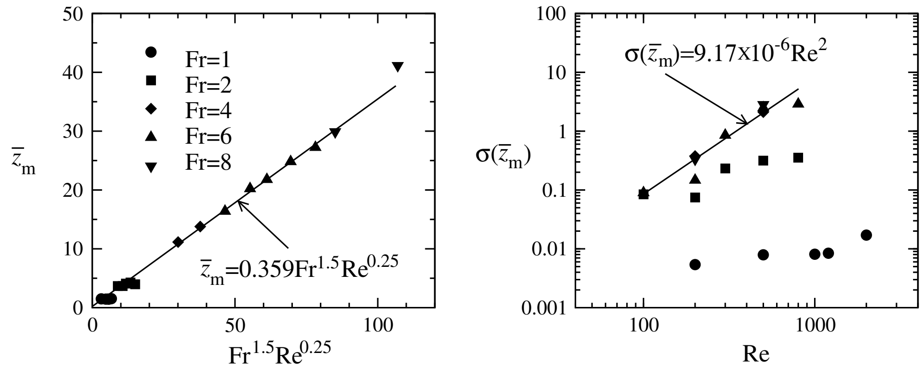

Fig. 15. (a) $\bar{z}_m$ plotted against $Fr^{3/2}Re^{1/4}$ and (b) $\sigma(\bar{z}_m)$ plotted against Re for all Fr and Re considered, where $\bar{z}_m$ is the time averaged value of z_m, the maximum penetration height of the fountain, at full development and $\sigma(\bar{z}_m)$ is its standard deviation. The straight line in (a) is the linear fit of the data represented by $\bar{z}_m = 0.359Fr^{3/2}Re^{1/4}$, and the straight line in (b) is the linear fit of the data represented by $\sigma(\bar{z}_m) = 9.17 \times 10^{-6}Re^2$ for $Fr > 2$.

4. Conclusions

The DNS results show that unsteady axisymmetric fountains in quiescent homogeneous ambient fluids with intermediate *Fr* and *Re* values ($1 \leqslant Fr \leqslant 8$ and $200 \leqslant Re \leqslant 800$) have the following transient flow behavior:

(a) At full development, entrainment at the upflow–downflow interface and at the downflow–ambient interface at a specific height *z* is well quantified by the respective standard deviations in the time series of r_u and r_w at *z* over a period of time at full development.

(b) For the $Fr = 1$ fountains, when $Re \leqslant 500$, it is found that the mean standard deviations are very small and are independent of *Re*, indicating that there is essentially no entrainment present at the interfaces. However, when $Re \geqslant 1000$, the mean standard deviations of both r_u and r_w are not trivial and increase substantially with *Re* (approximately in a power-law fashion), clearly showing that entrainment is present at both the upflow–downflow interface and the downflow–ambient interface and their extents increase with *Re*.

(c) *Re* has a large effect on r_u and r_w for the $Fr \geqslant 2$ fountains, especially when $Re \geqslant 500$, at which entrainment is present at the upflow–downflow interface, at the downflow–ambient interface and at the intrusion–ambient interface, with the extent increasing with *Re* (also approximately in a power-law fashion). However, when $Re \leqslant 200$, the *Re* effect diminishes even for *Fr* as high as 8, indicating that little entrainment is present at the upflow–downflow interface, at the downflow–ambient interface and at the intrusion–ambient interface. It is therefore concluded that *Re* has a predominant effect on entrainment present in fountain flows, whereas the affect from *Fr* is only secondary.

(d) The full development $\bar{z}_m$, which is the time averaged z_m, has an empirical relation with $Fr^{3/2}Re^{1/4}$, and its standard deviation, $\sigma(\bar{z}_m)$, increases monotonically with *Re* when $Fr > 2$, with an empirical relation with Re^2.

It should be noted that the quantitative dependence of the onset of entrainment on *Fr* and *Re* (especially the relation between *Fr* and the critical *Re* for the transition) can be, and should be, sought with much wider ranges of *Re* and *Fr* and with three-dimensional DNS in the future work. It is also crucial in the future work to develop quantitative entrainment coefficients to quantify the extent of entrainment present in these transitional fountains.

Acknowledgements

The authors acknowledge the support of the Australian Research Council. W. Lin also acknowledges the support of the 973 Program of China (Grant No. 2007CB216405), the National Natural Science Foundation of China (Grant No. 10262003), the Natural Science Foundation of Yunnan Province of China (Key Project, Grant No. 2003E0004Z), the Program for New Century Excellent Talents in University of China (Grant No. NCET-04-0918), and the JCU Faculty Grant Scheme.

References

[1] J.S. Turner, Jets and plumes with negative or reversing buoyancy, J. Fluid Mech. 26 (1966) 779–792.
[2] B.R. Morton, Forced plumes, J. Fluid Mech. 5 (1959) 151–163.
[3] B.R. Morton, The ascent of turbulent forced plumes in a calm atmosphere, Int. J. Air Poll. 1 (1959) 184–197.
[4] E.J. List, Turbulent jets and plumes, Ann. Rev. Fluid Mech. 14 (1982) 189–212.
[5] J.S. Turner, Turbulent entrainment: the development of the entrainment assumption, and its application to geophysical flows, J. Fluid Mech. 173 (1986) 431–471.
[6] B. Gebhart, Y. Jaluria, R.L. Mahajan, B. Sammakia, Buoyancy-Induced Flows and Transport, Hemisphere, New York, 1988.
[7] W.D. Baines, J.S. Turner, I.H. Campbell, Turbulent fountains in an open chamber, J. Fluid Mech. 212 (1990) 557–592.
[8] L.J. Bloomfield, R.C. Kerr, A theoretical model of a turbulent fountain, J. Fluid Mech. 424 (2000) 197–216.
[9] P.D. Friedman, J. Katz, Rise height for negatively buoyant fountains and depth of penetration for negatively buoyant jets impinging an interface, J. Fluids Eng. 122 (2000) 779–782.
[10] G.H. Jirka, Integral model for turbulent buoyant jets in unbounded stratified flows. Part I: single round jet, Environ. Fluid Mech. 4 (2004) 1–56.
[11] N.B. Kaye, G.R. Hunt, Weak fountains, J. Fluid Mech. 558 (2006) 319–328.
[12] H. Zhang, R.E. Baddour, Maximum penetration of vertical round dense jets at small and large Froude numbers, J. Hydraul. Eng. 124 (1998) 550–553.
[13] W. Lin, S.W. Armfield, The Reynolds and Prandtl number dependence of weak fountains, Comput. Mech. 31 (2003) 379–389.
[14] W. Lin, S.W. Armfield, Direct simulation of weak axisymmetric fountains in a homogeneous fluid, J. Fluid Mech. 403 (2000) 67–88.
[15] W. Lin, S.W. Armfield, Very weak fountains in homogeneous fluid, Numer. Heat Transfer, Part A: Appl. 38 (2000) 377–396.
[16] P. Philippe, C. Raufaste, P. Kurowski, P. Petitjeans, Penetration of negatively buoyant jet in a miscible liquid, Phys. Fluids 17 (2005) 053601.
[17] S.W. Armfield, Finite-difference solutions of the Navier–Stokes equations on staggered and non-staggered grids, Comput. Fluids 20 (1991) 1–17.
[18] S.W. Armfield, J.C. Patterson, Wave properties of natural-convection boundary layers, J. Fluid Mech. 239 (1992) 195–211.
[19] W. Lin, S.W. Armfield, Direct simulation of weak laminar plane fountains in a homogeneous fluid, Int. J. Heat Mass Transfer 43 (2000) 3013–3026.
[20] W. Lin, S.W. Armfield, Direct simulation of natural convection cooling in a vertical circular cylinder, Int. J. Heat Mass Transfer 42 (1999) 4117–4130.
[21] W. Lin, S.W. Armfield, Long-term behavior of cooling fluid in a vertical cylinder, Int. J. Heat Mass Transfer 48 (2005) 53–66.
[22] W. Lin, S.W. Armfield, J.C. Patterson, Cooling of a $Pr < 1$ fluid in a rectangular container, J. Fluid Mech. 574 (2007) 85–108.
[23] J.E. Simpson, Gravity Currents in the Environment and the laboratory, second ed., Cambridge University Press, New York, 1997.